Stable Perovskite Solar Cells based on Hydrophobic Triphenylamine Hole-Transport Materials

Xicheng Liu,[a, c] Lifeng Zhu,[b] Fei Zhang,[a] Jing You,*[a] Yin Xiao,[a] Dongmei Li,[b] Shirong Wang,[a] Qingbo Meng,[b] and Xianggao Li[a]

Two hole-transporting materials (HTMs) based on *N*,*N*,*N*′,*N*′-tetraphenylbenzidine (TPB) and MeO-triphenylamine (MOTPA) are synthesized. The HTMs offer outstanding thermal stability, film-forming properties, and hole mobilities. Perovskite solar cells (PSCs) are prepared using either pristine HTM layers or layers doped with cobalt salts. The nondoped PSCs with as-synthesized HTMs show better performance compared to *spiro*-OMeTAD, especially for long-time stability in ambient air. The power conversion efficiency (PCE) of the cells decreases by only 3% after 600 h of storage. The nondoped hole-transport layer (HTL) are hydrophobic, with a contact angle of 94.3° to water. The moisture-repelling ability of these HTMs are demonstrated by exposing the nondoped PSCs to an atmosphere saturated with water vapor. The PCE of doped PSCs with *spiro*-OMeTAD as HTL decreased 53%, while that of nondoped PSCs with the as-synthesized HTMs as HTL only decreased 27% after 15 min. These result thus show a new method to improve the operational stability of PSCs, especially at high humidity levels.

Introduction

Very recently, the power conversion efficiency (PCE) of hybrid organic–inorganic perovskite ($CH_3NH_3PbX_3$, where X corresponds to halogen) solar cells (PSCs) was reported to exceed 20%.[1] PSCs are considered to be the most promising technology for the next generation of photovoltaic devices owing to merits such as simple fabrication processes, low costs, and outstanding performance. Unfortunately achieving long-term stability is still a major challenge, especially when operating in high-humidity environments.

The mechanism of PSC degradation has been investigated by many groups, and there are three components contributing to the degradation: moisture and oxygen effects, thermal effects, and the effects of exposure to ultraviolet (UV) light.[2] The thermal effects mainly affect the crystal form.[3] Without oxygen and moisture, thermal effects on the performance of solar cells are negligible.[4] UV exposure leads to a decrease of the PCE owing to the recombination of holes with electrons generated by excitation of TiO_2 nanoparticles. The decomposition mechanism of $CH_3NH_3PbI_3$ perovskite layers in moist circumstances can be mainly ascribed to the reaction shown in Equation (1).[5] PbI_2 dissolves out of the perovskite's hole transport layers, resulting in a porous structure that in turn further accelerates the decomposition process by increased moisture absorption.

$$4\,CH_3NH_3PbI_3 + 2\,H_2O \rightarrow (CH_3NH_3)_4PbI_6 \cdot 2\,H_2O + PbI_2 \quad (1)$$

In the mesoporously structured PSCs, the hole transport layer (HTL) between the perovskite layer and the cathode acts as electron-blocker, transports holes to the cathode, and enhances charge separation at its interface to the perovskite layer.[6] Among such hole transport materials (HTMs), 2,2′,7,7′-tetrakis(*N*,*N*′-di-*p*-methoxy-phenylamine)-9,9′-spirobifluorene (*spiro*-OMeTAD) has been shown to highly effective, but a high density of large pinholes is present in lithium-salt-doped and cobalt-salt-doped *spiro*-OMeTAD layers, which is detrimental to the organic lead perovskite.[7] In our previous report, small-molecule HTMs based on triphenylamine (TPA) showed a higher PCE without doping.[8]

Herein, in order to improve the thermal stability and film-forming ability, we synthesize two small-molecule HTMs based on tetraphenylbenzidine and MeO-triphenylamine (TPB-*n*-MOTPA, $n = 2$, 4, Figure 1). Interfacial carrier transfer processes are studied by time-resolved photoluminescence (PL) measurements, and reveal that TPB-*n*-MOTPA

[a] X. Liu, F. Zhang, Dr. J. You, Y. Xiao, Prof. Dr. S. Wang, Prof. Dr. X. Li
Department of Applied Chemistry
School of Chemical Engineering and Technology
Tianjin University
Collaborative Innovation Center of Chemical Science and Engineering (Tianjin)
92 Weijin Str., Nankai Dist., Tianjin 300072 (PR China)
E-mail: youj1983@tju.edu.cn

[b] L. Zhu, Prof. Dr. D. Li, Prof. Dr. Q. Meng
Key Laboratory for Renewable Energy (CAS)
Beijing Key Laboratory for New Energy Materials and Devices
Beijing National Laboratory for Condense Matter Physics
Institute of Physics, Chinese Academy of Sciences
8 South-three Str., Zhongguancun, Beijing 100190 (PR China)

[c] X. Liu
School of Chemistry and Chemical Engineering
Qufu Normal University
57 Jingxuan West Str., Qufu 273165 (PR China)

Supporting Information for this article can be found under: http://dx.doi.org/10.1002/ente.201600303.

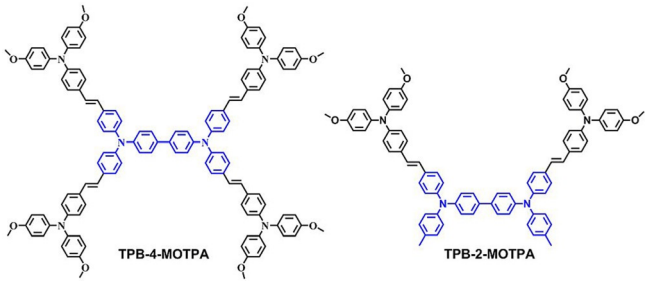

Figure 1. Molecular structures of TPB-2-MOTPA and TPB-4-MOTPA.

HTMs have excellent charge-transfer and electron-blocking properties. Spin-coated TPB-*n*-MOTPA thin films show good hydrophobicity. The compacted surfaces were investigated by atomic force microscopy (AFM). The nondoped mesoporously structured PSCs prepared by using TPB-2-MOTPA achieve PCE values of up to 11.06%. The PCE values of PSCs fabricated with TPB-2-MOTPA decrease less than 3% after 600 h of storage. The moisture-tolerance properties of these HTMs were investigated by exposing the nondoped PSCs to an atmosphere saturated with water vapor. The PCE of doped PSCs with *spiro*-OMeTAD as HTL decreased by 53%, while the PCE of nondoped PSCs using our as-synthesized HTMs as HTL only decreased by 27% after 15 min. This result shows a new method to improve the operational stability of PSCs, especially at high humidity levels.

Results and Discussion

Synthesis of TPB-n-MOTPA

TPB-*n*-MOTPA samples were obtained from Wittig reactions in yields of >70%. The glass-transition temperatures (T_g) and decomposition temperatures (T_d) of the samples were determined by differential scanning calorimetry (DSC) and thermal gravimetric analysis (TGA), respectively (Supporting Information, Figure S2). As shown in Table 1, the outstanding thermal stability of the TPB-*n*-MOTPAs was confirmed by the higher T_g and T_d values compared to most other reported small-molecule HTMs.[9]

UV/Vis absorption spectra of the TPB-*n*-MOTPAs in dilute tetrahydrofuran (THF) solution (1.0×10^{-5} mol L^{-1}) and as solid films are shown in Figure 2. There are two obvious sets of absorption peaks in both *spiro*-OMeTAD and the TPB-*n*-MOTPAs. The peaks at short wavelengths can be assigned to n–π* transition of the TPA moiety, while the peaks at longer wavelengths can be assigned to intramolecular charge transfer (ICT) of π–π*.[10] These three compounds show similar n–π* transition peaks, while the ICT peaks show bathochromic shifts from *spiro*-OMeTAD to TPB-*n*-MOTPA owing to the extension of π–π conjugated structures.[11] That there were obvious changes in the absorption spectra of the thin films indicates that the spin-coated films are amorphous, which was further confirmed by X-ray diffraction (XRD) measurements (Supporting Information, Figure S4).[12] Slight bathochromic shifts (5 nm, 3 nm and 2 nm for TPB-4-MOTPA, TPB-2-MOTPA, and *spiro*-OMeTAD,

Table 1. Optical, electrochemical, and thermal properties, and energy levels of TPB-*n*-MOTPA.

Sample	λ_{onset}[a] [nm]	λ_{abs}[a] [nm]	E_g[b] [eV]	HOMO[c] [eV]	LUMO[d] [eV]	T_g[e] [°C]	T_d[f] [°C]
TPB-4-MOTPA	457	299, 408/ 302, 413[g]	2.71	−5.25	−2.54	151.0	431.8
TPB-2-MOTPA	447	301, 404/ 309, 407[g]	2.77	−5.28	−2.51	117.5	416.1

[a] Absorption spectra recorded in 1.0×10^{-5} mol L^{-1} THF solution. [b] Optical energy gaps calculated by the absorption thresholds (λ_{onset}) from UV/Vis absorption spectra of films. [c] Measured with photoelectron yield spectroscopy (PYS, Supporting Information, Figure S3). [d] $|LUMO| = |HOMO| - |E_g|$. [e] Decomposition temperatures measured by TGA at a heating rate of 10 °C min^{-1} under N_2. [f] Measured by DSC at a heating rate of 10 °C min^{-1} under N_2 according to the heat-cool-heat procedure. [g] Absorption peaks of solid films.

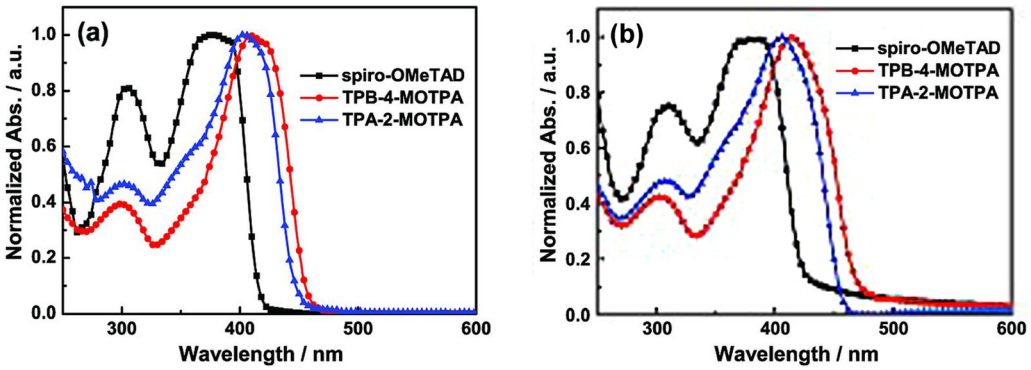

Figure 2. UV/Vis absorption spectra of TPB-*n*-MOTPAs and *spiro*-OMeTAD. a) THF solution ($c=1.0\times10^{-5}$ mol L^{-1}), b) solid films.

respectively) and broadening of the ICT bands is observed, which indicates minor intermolecular interactions in the solid state.[13]

The optimized molecular structures and frontier molecular orbital distribution of TPB-*n*-MOTPA and *spiro*-OMeTAD were studied by density functional theory (DFT) calculations (Figure 3).[14] In TPB-*n*-MOTPAs, the highest occupied molecular orbitals (HOMO) are distributed over the entire molecular skeleton. The π–π conjugation network of TPB-4-MOTPA is larger than of TPB-2-MOTPA, which contributes to a higher HOMO level for the former. The lowest unoccupied molecular orbital (LUMO) is mainly distribute on the TPB units. Similar to *spiro*-OMeTAD, the TPB center of the TPB-*n*-MOTPAs adopts a *spiro* conformation because of the larger MOTPA terminal branches. At the ends of both molecules, the propeller-shaped MOTPA derivatives give the same type of distortion. The measured angles between the two MOTPA branches in TPB-*n*-MOTPAs are 64.91° and 65.75°, as compared to 89.94° between the two fluorine rings in *spiro*-OMeTAD, which is consistent with an earlier literature report.[15] The *spiro* conformation of the TPB-*n*-MOTPAs will prevent strong intermolecular stacking and lead to formation of amorphous solid films.

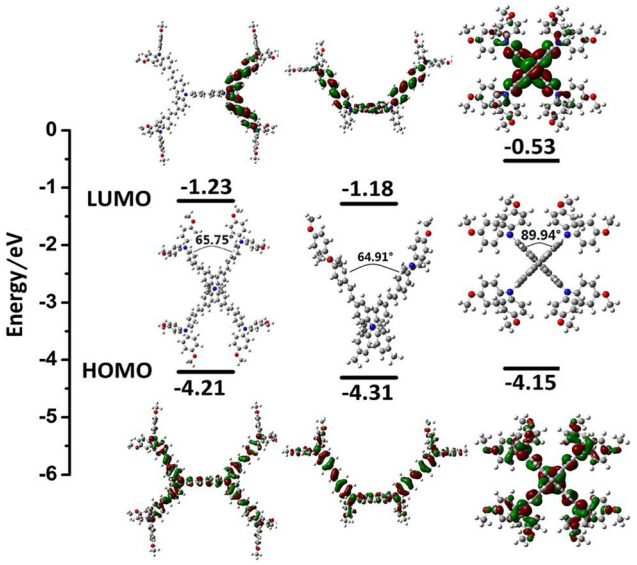

Figure 3. HOMO and LUMO distributions and optimized molecular structures of TPB-*n*-MOTPA ($n=2,4$) and *spiro*-OMeTAD.

Time-of-flight (TOF) transient hole-current measurements were used to measure the hole mobilities of the HTMs (Supporting Information, Figure S5). At room temperature, the hole mobilities of TPB-4-MOTPA and TPB-2-MOTPA are 7.4×10^{-5} and 7.7×10^{-5} $cm^2V^{-1}s^{-1}$, respectively, at an applied electric field of 2.0×10^5 Vcm^{-1}. Under the same conditions, the hole mobility of *spiro*-OMeTAD was 5.0×10^{-4} $cm^2V^{-1}s^{-1}$.

Application in mesoporous perovskite solar cells

The structures of PSCs and their energy levels are shown in Figure 4. The HOMO levels match well to the valence band level of the organometallic halide $CH_3NH_3PbI_3$ (−5.43 eV), favoring hole transfer. The LUMO levels of the TPB-*n*-MOTPAs are much higher than the conduction band level of $CH_3NH_3PbI_3$ (−3.93 eV) to block back-transfer of electrons from $CH_3NH_3PbI_3$ to the gold electrode (Figure 4b).[8]

The device structure was investigated by using high-resolution cross-sectional scanning electron microscopy (SEM; Figure 4a). The perovskite layer was prepared by using a two-step sequential method, as described in the literature.[16] The complete conversion of PbI_2 to $CH_3NH_3PbI_3$ was identified by its XRD pattern (Supporting Information, Figure S6).

In order to investigate the effect of the hole transport layers (HTLs), mesoporously structured PSCs were fabricated using HTMs doped with 5% Co^{III}TFSI [HTM (D)], and using pristine HTMs. Current-voltage (*J–V*) curves and incident photon-to-electron conversion efficiency (IPCE) spectra are shown in Figure 5, while the corresponding parameters are shown in Table 2.

The PSCs with HTLs showed improved short-circuit current density (J_{sc}) values and open circuit voltages (V_{oc}) compared to devices without a HTL. Interestingly, the nondoped PSCs showed an enhancement factor with a profile corresponding to the absorption spectra of the of HTMs (Fig-

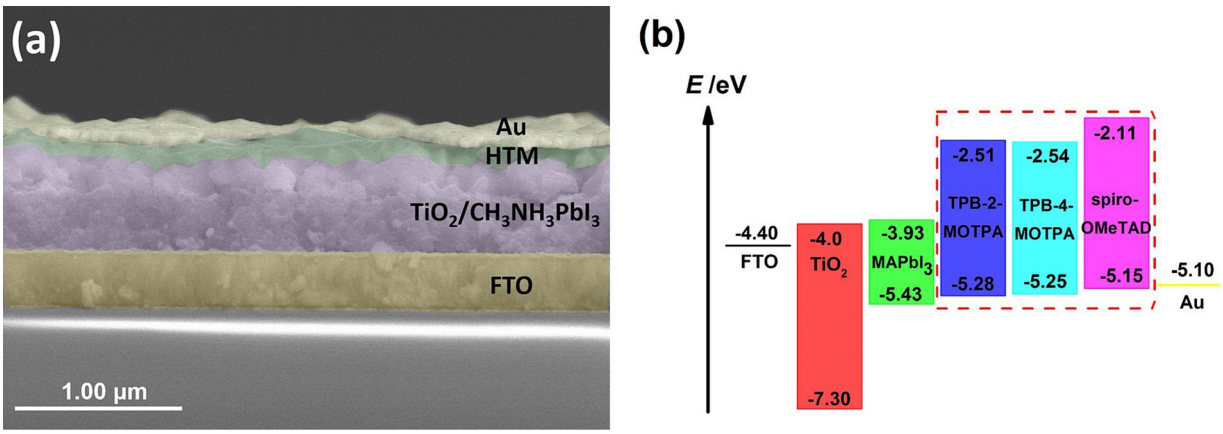

Figure 4. a) Schematic, and b) energy level diagram of the perovskite solar cells based on HTMs.

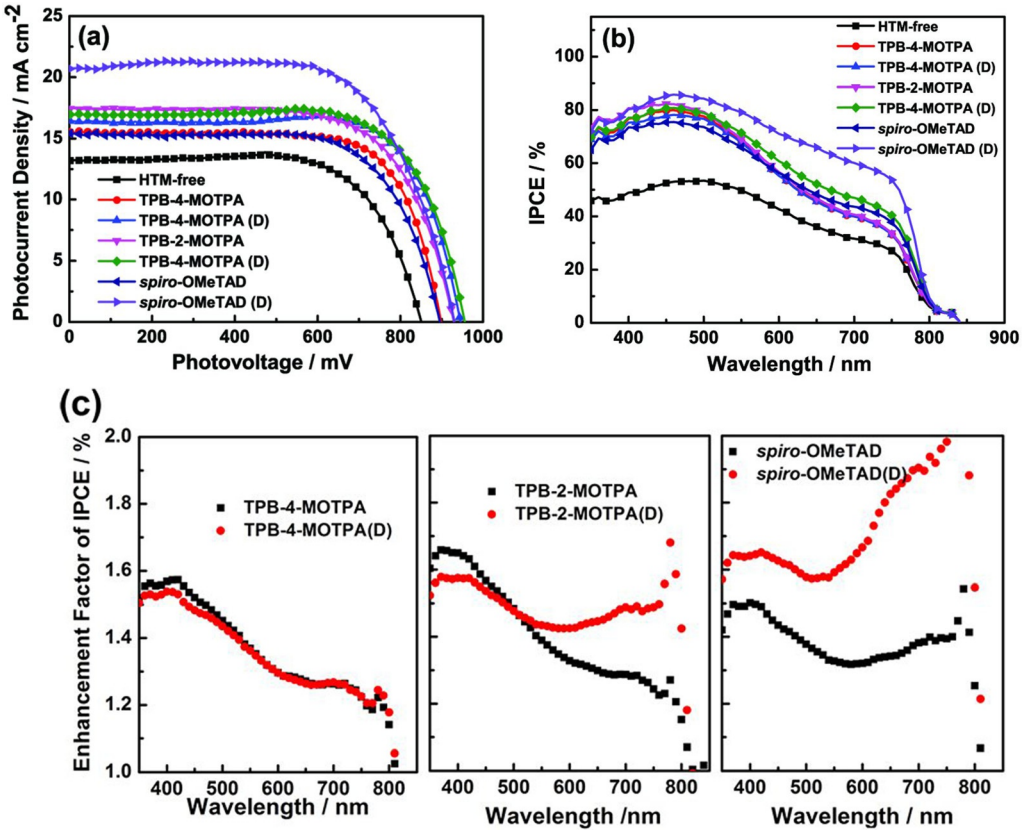

Figure 5. a) *J–V* curves, and b) IPCE spectra of $TiO_2/CH_3NH_3PbI_3$/HTM/Au solar cells (HTM = TPB-*n*-MOTPA, *spiro*-OMeTAD) and the $TiO_2/CH_3NH_3PbI_3$/Au solar cells. c) IPCE enhancement factor, determined by the ratio of PSC with and without HTL, in which red discs represent nondoped type, black discs represent doped one.

Table 2. Device parameters of PSCs under AM 1.5 illumination (100 mW cm^{-2}).

HTMs	J_{sc}[a] [mA cm^{-2}]	V_{oc} [mV]	*FF*	PCE [%]
HTM-free	13.23/10.77	854.4	0.70	7.88
TPB-4-MOTPA	15.49/14.72	896.2	0.73	10.10
TPB-4-MOTPA (D)	16.41/14.61	948.5	0.74	11.55
TPB-2-MOTPA	17.37/15.90	927.6	0.69	11.06
TPB-2-MOTPA (D)	16.98/15.10	958.9	0.71	11.62
spiro-OMeTAD	15.41/14.81	895.2	0.70	9.61
spiro-OMeTAD (D)	20.03/18.34	921.1	0.72	13.28

[a] Obtained by integration of IPCE spectra. The reproducibility of the cells' performance based on TPB-*n*-MOTPA is evaluated by testing photovoltaic parameters of twenty cells. Related data are presented in Supporting Information, Table S2.

ure 5c). For the doped PSCs, the enhancement at longer wavelengths were more pronounced, except for the PSCs doped with TPB-4-MOTPA. The poor dispersion of Co^{III}TFSI in TPB-4-MOTPA resulted in no obvious improvements to the IPCE for these doped PSCs. The IPCE enhancements indicate that PSCs with nondoped TPB-*n*-MOTPAs exhibit improved light-utilization efficiencies.

As shown in Table 2, the PSCs based on *spiro*-OMeTAD doped with Co^{III}TFSI show larger J_{sc}, V_{oc}, *FF*, and PCE values than the nondoped ones. However, the doped PSCs showed only slightly increases for TPB-*n*-MOTPAs compared to the nondoped ones. The PSCs with TPB-*n*-MOTPAs show larger V_{oc} values than *spiro*-OMeTAD, which is in line with their deeper-lying HOMO levels.[8]

There were obvious improvements in the photocurrents generated by excitation of the $CH_3NH_3PbI_3$ layer. The HTLs mainly improved the charge separation and collection at the interface. This process can be identified by measuring time-resolved PL decay curves of the PSCs. As shown in Figure 6a, illumination by a 445 nm laser excites the $CH_3NH_3PbI_3$ layer. The energy is released through radiative decay (emitting at 775 nm), nonradiative decay, and charge separation, with their rate constants denoted as k_r, k_{nr}, and k_{CT}, respectively. The PL decay lifetime (τ_{PL}) of $CH_3NH_3PbI_3$ can be expressed as $\tau_{PL} = 1/(k_r + k_{nr} + k_{CT})$. The τ of samples $CH_3NH_3PbI_3$, $CH_3NH_3PbI_3$/TPB-*n*-MOTPA (D) and $CH_3NH_3PbI_3$/*spiro*-OMeTAD (D) films were determined by their decay profile at 775 nm (Figure 6b).[17] For the $TiO_2/CH_3NH_3PbI_3$ film without a HTM layer, τ_{PL} was 167.74 ns. When a thin HTM layer was coated on the surface of $CH_3NH_3PbI_3$, τ_{PL} significantly decreased, to 63.71 ns for $CH_3NH_3PbI_3$/*spiro*-OMeTAD, 72.22 ns for $CH_3NH_3PbI_3$/TPB-4-MOTPA, and 21.82 ns for $CH_3NH_3PbI_3$/TPB-2-MOTPA. This is due to the HTLs improving the charge separation process (k_{CT}). The short lifetime of sample $CH_3NH_3PbI_3$/TPB-2-MOTPA suggests that TPB-2-MOTPA

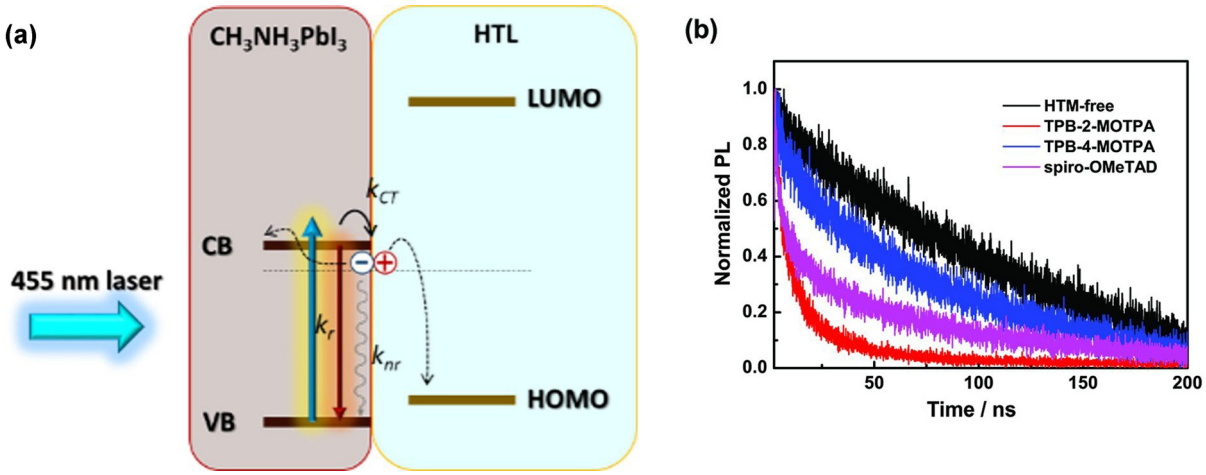

Figure 6. Time-resolved PL spectra of $TiO_2/CH_3NH_3PbI_3$, $TiO_2/CH_3NH_3PbI_3$/TPB-*n*-MOTPA and $TiO_2/CH_3NH_3PbI_3$/*spiro*-OMeTAD films, monitored at 775 nm during the transformation. Excitation wavelength: 445 nm.

improves charge separation the most, compared to *spiro*-OMeTAD and TPB-4-MOTPA. This should be the reason why PSCs based on TPB-2-MOTPA showed the best performance among the nondoped devices.

Stability and lifetime of perovskite solar cells

The long-term stability of PSCs, especially in ambient air, is an issue with regard to their potential application. Because PSCs based on TPB-2-MOTPA showed the best performance, so compared their to PSCs using *spiro*-OMeTAD. The operational stability was investigated by measuring the *J*–*V* curves after storage under atmospheric conditions at 24 h intervals. The time-dependent change ratios are shown in Figure 7. Generally speaking, the PCE only decreased $<10\,\%$ after 600 h of storage. The decreases of J_{sc} and *FF* were more obvious, while V_{oc} was unchanged. In the first 300 h, a slight increase of J_{sc} was observed nondoped PSCs with TPB-2-MOTPA and *spiro*-OMeTAD, as well as the doped PSC with TPB-2-MOTPA. For the long storage times (300–600 h), the decreases of J_{sc} in the doped PSCs are more obvious. This indicated that nondoped PSCs based on TPB-2-MOTPA have promising long-term stabilities at room temperature.

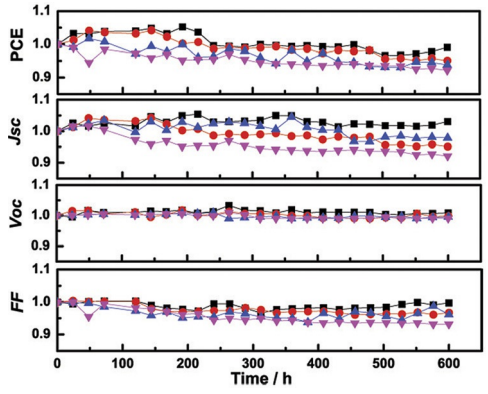

Figure 7. PCE, J_{sc}, V_{oc}, and *FF* of perovskite solar cells with TPB-2-MOTPA and *spiro*-OMeTAD versus storage time. (■ TPB-2-MOTPA; ● TPB-2-MOTPA(D); ▲ *spiro*-OMeTAD; ▼ *spiro*-OMeTAD(D)).

As shown in Equation (1), the decomposition of $CH_3NH_3PbI_3$ is one of the most important factors in the degradation of PSCs. This degradation can be monitored by changes in the XRD patterns.[18] The XRD patterns of PSCs based on *spiro*-OMeTAD and TPB-2-MOTPA at ca. 40 % humidity are shown in Figure 8. The two sharp peaks at 14.2° and 28.5° can be assigned to the $CH_3NH_3PbI_3$ layer, which was unchanged in all PSCs after 450 h of storage. On the other hand, after storage of the doped PSCs a weak peak appeared at 12.2° (Figure 8a and b). For doped PSCs with *spiro*-OMeTAD the peak appeared after 250 h of storage, compared to 400 h for TPB-2-MOTPA. This indicates that decomposition occurs much faster in doped PSCs. As reported, when *spiro*-OMeTAD is doped with lithium or cobalt salts, pinholes are unavoidable in films fabricated by spin-coating, and this is considered to be the main reason behind the decomposition of $CH_3NH_3PbI_3$ layers in mesoporous PSCs.[19]

Atomic force microscopy (AFM) images of doped *spiro*-OMeTAD and TPB-2-MOTPA are shown in Figure 9a and b. In both cases, pinholes are obvious. In the doped TPB-2-MOTPA film, the numbers of pinholes is lower than in the case of the doped *spiro*-OMeTAD films. In nondoped HTLs a smooth compact surface is apparent in the AFM images (Figure 9c and d). As reported for, for example, poly(3-hexylthiophene) (P3HT),[20] smooth compact HTLs can act as a barrier for moisture ingress. The contact angles (θ) between H_2O and the HTLs were measured to investigate their hydrophobicity. The inserts Figure 8 reveal that the θ value of nondoped TPB-2-MOTPA is 94.3°, higher than that of *spiro*-OMeTAD (81.2°). The θ dramatically decreased after doping with cobalt ions. This might be the cause of higher stability for long-term storage in nondoped PSCs.

The ability of the nondoped HTLs to deal with moisture was investigated by putting PSCs into containers fully filled with water vapor for 15 and 30 min, and then measuring

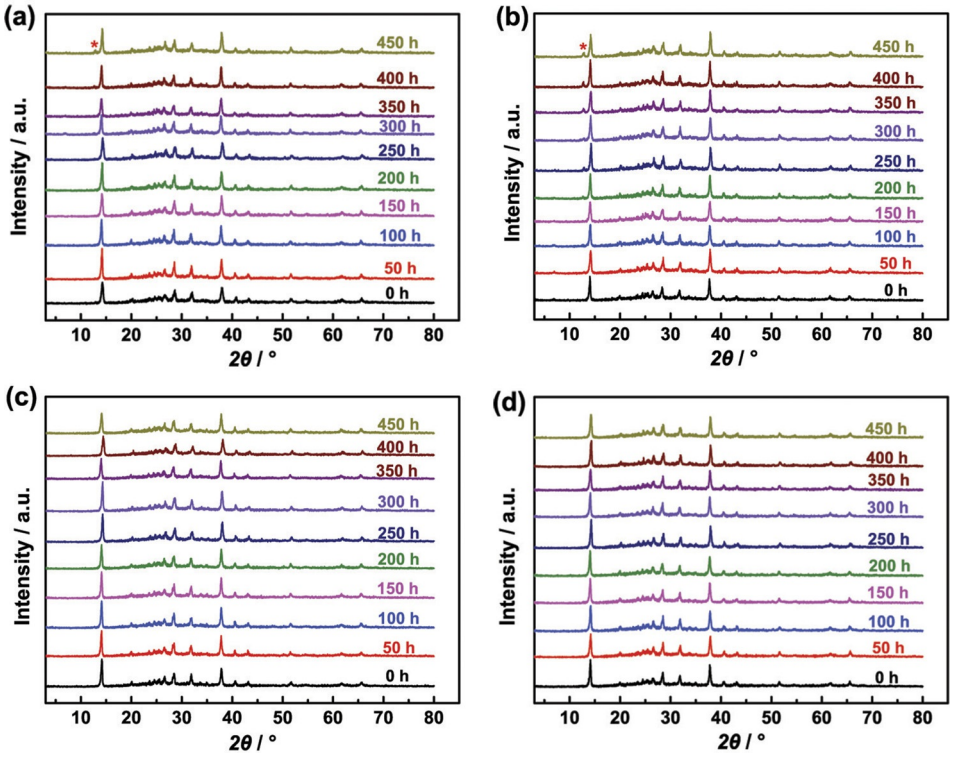

Figure 8. XRD patterns of devices with HTM-doped and HTM-pristine which were exposed to ca. 40% relative humidity after 450 h exposure: a) TPB-2-MOTPA doped; b) *spiro*-OMeTAD doped; c) TPB-2-MOTPA pristine; d) *spiro*-OMeTAD pristine. (★ denotes the peaks of PbI_2).

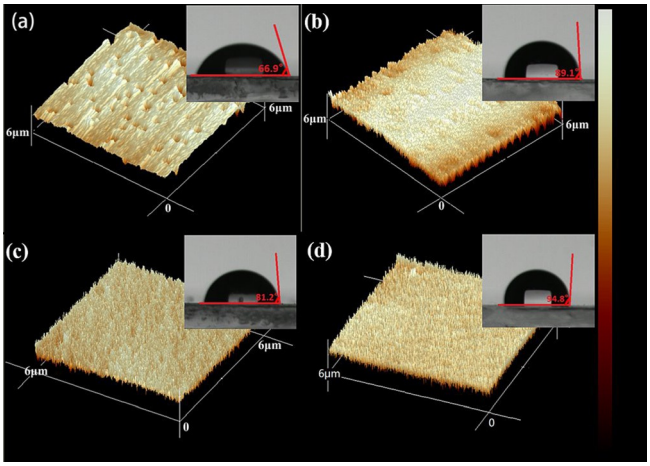

Figure 9. AFM images of HTMs doped and pristine films (insets are the contact angles between HTMs and water): a) *spiro*-OMeTAD doped; b) TPB-2-MOTPA doped; c) *spiro*-OMeTAD pristine; d) TPB-2-MOTPA pristine.

their current–voltage curves. As shown in Figure 10, when exposed to water vapor for 15 min, the decrease of J_{sc}, *FF*, V_{oc}, and PCE for *spiro*-OMeTAD doped PSCs is 12, 39, 17, and 53%, respectively. When PSCs based on doped *spiro*-OMeTAD were exposed to water vapor for 30 min, the decrease of J_{sc}, *FF*, V_{oc}, and PCE were 52, 39, 35, and 81%, respectively. However, the decreases of J_{sc}, *FF*, V_{oc}, and PCE for TPB-2-MOTPA nondoped PSCs with exposure time of 15 and 30 min are 11, 19, 0, 27% and 31, 41, 6, 61%, respectively. The moisture-induced degradation of doped PSCs is much faster than nondoped PSCs. Notably, the decrease of V_{oc} in doped PSCs is more obvious after extending the exposure time owing to decomposition of the $CH_3NH_3PbI_3$ layer. This tendency is suppressed in nondoped PSCs with TPB-2-MOTPA as HTL, which can be attributed to the outstanding hydrophobicity and compactness of the nondoped TPB-2-MOTPA layer. As discussed above, the nondoped TPB-2-MOTPA shows a moisture handling ability that can protect PSCs from degradation of PSCs, even in a high-humidity atmosphere.

Conclusions

Two TPB-based *spiro*-type hole transport materials (HTMs; TPB-4-MOTPA and TPB-2-MOTPA) are synthesized by an easy method. The HOMO and LUMO energy levels of these TPB derivatives are effectively tuned to match to the perovskite by adjusting the molecular conjugated network, which is confirmed by optical and electrochemical studies, and theoretical calculations. Nondoped perovskite solar cells (PSCs) based on TPB-4-MOTPA and TPB-2-MOTPA as HTMs afford power conversion efficiencies of 10.10% and 11.06%, respectively, which compare favorably to nondoped PSCs based on *spiro*-OMeTAD. The nondoped PSCs show a better stability after 600 h of storage in atmospheric conditions, owing to the smooth and compact surface morphology of nondoped HTLs which prevents the action of moisture. The moisture-repelling feature of the HTLs is demonstrated by

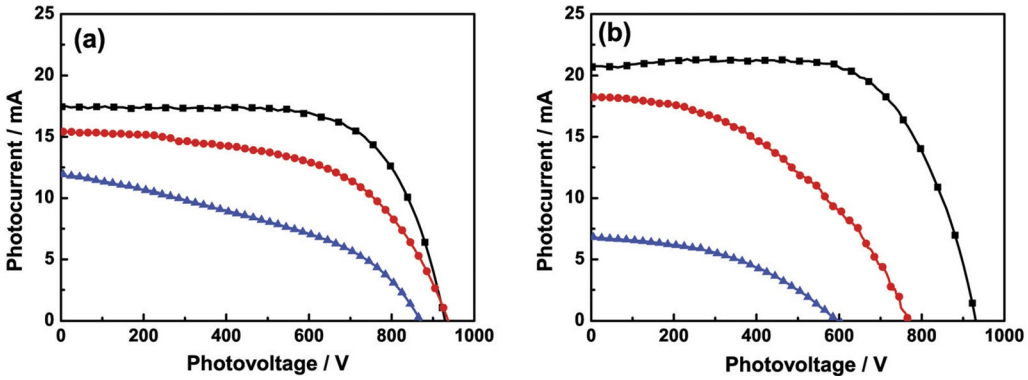

Figure 10. *J–V* curves of Non-doped PSCs with TPB-2-MOTPA as HTL a) and doped PSCs with *spiro*-OMeTAD as HTL b) exposure in water vapor for 0 min (black line), 15 min (red line) and 30 min (blue line).

exposing the nondoped PSCs to an atmosphere fully saturated with water vapor. After 15 min, the power conversion efficiency (PCE) of nondoped PSCs with *spiro*-OMeTAD decreased by 53%, while that of nondoped PSCs with as-synthesized HTMs only decreased by 27%. This result shows a new method to improve the operational stability of PSCs, especially at high humidity levels.

Experimental Section

Materials

N,*N*,*N*′,*N*′-Tetraphenylbenzidine (TPB) and *N*,*N*′-Diphenyl-*N*,*N*′-di(*p*-tolyl)benzidine (*p*-TPD) were purchased from Heowns Biochemical Technology Co. Ltd., Tianjin, China. PbI_2 was purchased from Aldrich, *N*,*N*′-dimethylformide (DMF) from Alfar Aesar, hydroiodic acid (AR, 45 wt% in water) and methylamine (AR, 27% in methanol) from Sinopharm Chemical Reagent Co. Ltd. 2,2′,7,7′-Tetrakis (*N*,*N*-di-*p*-methoxyphenylamine)-9,9′-spirobifluorene (*spiro*-OMeTAD) was from Luminescence Technology Corp., Taiwan, China. Tetrahydrofuran was distilled before use, all the other agents were directly used without further purification. Methyl ammonium iodide (CH_3NH_3I) was prepared according to a reported procedure.[21] Substrates were FTO conducting glass (Pilkington, thickness: 2.2 mm, sheet resistance: 14 Ω/□). Patterned FTO glass was first cleaned with mild detergent, rinsed several times with distilled water and subsequently with ethanol in an ultrasonic bath, and finally dried under air stream.

Measurements

TPB-*n*-MOTPA was identified by nuclear magnetic resonance (NMR) spectrometry and mass spectrometry (MS). NMR spectra were obtained on a Bruker AVANCE III 400 MHz instrument, with the chemical shifts reported in ppm using tetramethylsilane (TMS) as an internal standard. MS were measured on a LCQ Advantage MAX mass spectrometer. UV/Vis spectroscopy was performed on a Thermo Evolution 300 UV/Visible spectrometer. The decomposition temperature (T_d) and glass transition temperature (T_g) were determined by thermogravimetric analysis (TGA) and differential scanning calorimetry (DSC) on a TA Q500 thermo gravimetric analysis and TA Q20 thermal analysis instrument under a nitrogen atmosphere. Photoelectron yield spectroscopy (PYS) was carried out on a Sumitomo PYS-202 ionization energy detection system. X-ray diffraction (XRD) was measured by using a Rigaku Miniflex 600 X-Ray diffraction instrument. Scanning electron microscopy (SEM) was measured by using a Hitachi S-4800.

Current–voltage characteristics (*J–V*) were measured on a Keithley 2602 SourceMeter under AM 1.5 irradiation (100 mW cm^{-2}) from an Oriel Solar Simulator 91192. A mask with a window of 0.08 cm^2 was clipped onto the TiO_2 side to define the photoactive area of the cells. The incident-photon-to-current conversion efficiency (IPCE) was measured by the direct current (DC) method using a lab-made IPCE setup under 0.3–0.9 mW cm^{-2} monochromic light illumination without bias illumination.[22] Time-resolved PL spectra were recorded on an Edinburgh Instruments FLS 900 PL spectrometer, excited with a picosecond pulsed diode laser (EPL-445), and measured at 775 nm after excitation at 445 nm. The time-of-flight (TOF) measurements were recorded on a TOF401 measurement system, Sumitomo Heavy Industries. Ltd. Samples were prepared by spin-coating with a structure of ITO/as-synthesized compounds (ca. 1 μm)/Al (100 nm), with a working area of 3 × 3 mm^2.

Synthesis

The synthetic routes towards TPB-*n*-MOTPA are shown in Scheme 1. TPB-*n*-MOTPA samples were synthesized by Wittig reactions using formyl-replaced tetraphenylbenzidine (**3**,**4**) and Wittig reagents (**5**) in three steps from commercially available and relatively inexpensive starting reagents. The structures of the as-synthesized compounds were confirmed via ^{1}H NMR and MS, and agreed well with the proposed molecular structures (see Supporting Information, Figure S1).

Synthesis of N,N,N′,N′*- tetra(4-formylphenyl)-1,1′-biphenyl-4,4′-diamine (3)*[23]

TPB (5.0 g, 10.2 mmol) and imidazole (5.1 g, 61.5 mmol) were added into a two-neck 250 mL round bottom flask, followed by 90 mL of acetonitrile. Trifluoroacetic anhydride (17.3 mL, 0.123 mol) was added dropwise in a nitrogen atmosphere (N_2). The mixture was refluxed until TPB was consumed completely (monitored by thin-layer chromatography). The reaction solution was poured into 1 L of water to dissolve out precipitate a yellow powder. The filter cake washed with water until the filtrate became colorless, and product **1** was obtained: yellow solid

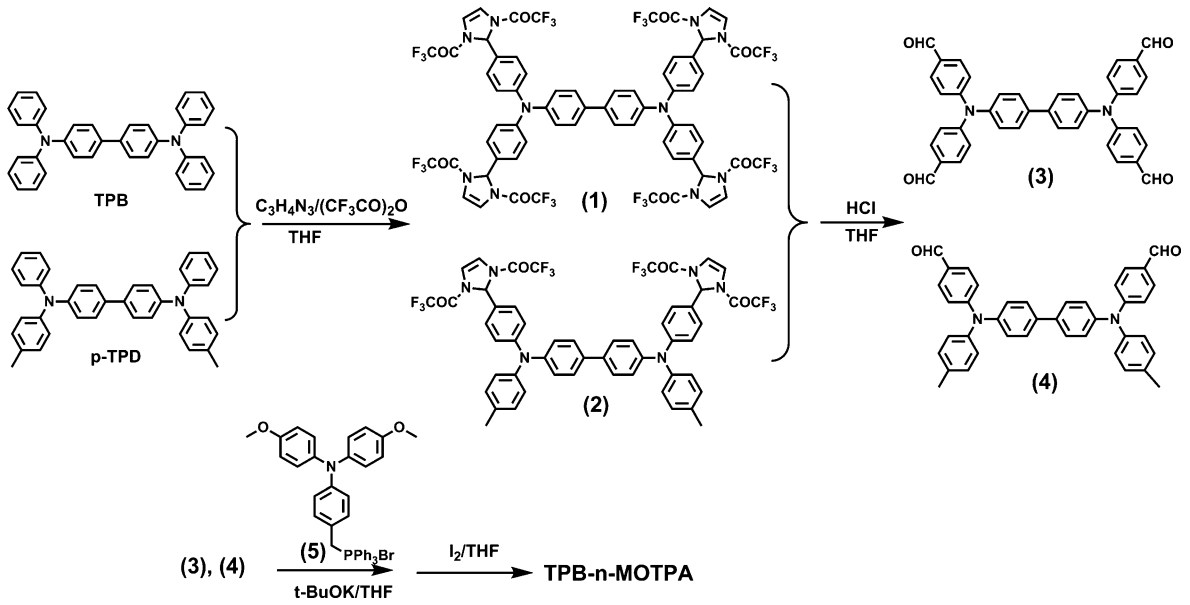

Scheme 1. Synthetic routes towards TPB-*n*-MOTPAs.

(15.4 g, 98.3 %); ^{1}H NMR (400 MHz, $CDCl_3$): δ = 7.49 (d, J = 8.5 Hz, 4H, Ar H), 7.37 (d, J = 8.6 Hz, 8H, Ar H), 7.21–6.99 (m, 16H, Ar H), 6.71 ppm (s, 8H,=CH); MS (m/z) [M^-] Calcd for $C_{64}H_{36}F_{24}N_{10}O_8$, 1528.2; Found, 1528.0.

The polyimidazoline product (10 g, 6.5 mmol) was dissolved in 200 mL THF. Then pumped HCl gas (100 mL, 2.5 mol L−1—prepared by adding 21.0 mL of concentrated HCl to 79.0 mL H2O). The reaction solution was refluxed for 12 h. The reaction solution was cooled to room temperature, and an orange solid formed. The reaction mixture was filtered and recrystallized from diethyl ether, and compound **3** was obtained (3.8 g, 96.0 %): mp 181–182 °C, 1H NMR (400 MHz, $CDCl_3$): δ = 9.93 (d, J = 11.8 Hz, 4H, CHO), 7.83 (t, J = 11.7 Hz, 8H, Ar H), 7.63 (t, J = 8.1 Hz, 4H, Ar H), 7.32–7.18 ppm (m, 13H, Ar H); MS (m/z) [M+H]$^+$: calcd for $C_{40}H_{28}N_2O_4$, 601.2; found, 601.4.

N,N′-*di*(p-tolyl)-N,N′-*di*(p-phenylbenzaldehyde)-1,10-biphenyl-4,4′-diamine (4) was synthesized using the same method

Compound **2**: ^{1}H NMR (400 MHz, $CDCl_3$): δ = 7.44 (d, J = 8.3 Hz, 4H, Ar H), 7.29 (t, J = 8.7 Hz, 4H, Ar H), 7.19–6.97 (m, 18H, Ar H), 6.70 (d, J = 10.4 Hz, 4H,=CH), 2.35 ppm (d, J = 11.8 Hz, 6H, CH_3); MS (m/z) [M^-]: calcd for $C_{52}H_{36}F_{12}N_6O_4$, 1036.3; found, 1036.2.

N,N′-di(*p*-tolyl)-*N,N′*-di(*p*-phenylbenzaldehyde)-1,10-biphenyl-4,4′-diamine (**4**): 91 %; Mp. 190–191 °C; ^{1}H NMR (400 MHz, $CDCl_3$): δ = 9.80 (s, 2H, CHO), 7.68 (d, J = 8.6 Hz, 4H, Ar H), 7.52 (d, J = 8.4 Hz, 4H, Ar H), 7.20 (dd, J = 13.9, 8.3 Hz, 8H, Ar H), 7.14–7.07 (m, 4H, Ar H), 7.04 (d, J = 8.6 Hz, 4H, Ar H), 2.35 ppm (d, J = 12.3 Hz, 6H, CH_3); MS (m/z) [M+H]$^+$: calcd for $C_{40}H_{32}N_2O_2$, 573.2; found, 573.2.

Synthesis of 4-[N,N-*di*(4-methoxyphenyl)amino]benzyl(triphenyl)-phosphonium bromide (5)

Wittig reagents (**5**) were synthesized according to literature:[10] ^{1}H NMR (400 MHz, $CDCl_3$): δ = 7.82–7.59 (m, 15H), 6.96 (d, J = 8.9 Hz, 4H, Ar H), 6.81 (dd, J = 11.1, 5.6 Hz, 6H, Ar H), 6.64 (d, J = 8.4 Hz, 2H, Ar H), 5.20 (d, J = 13.5 Hz, 2H, CH_2), 3.77 ppm (s, 6H, OCH_3); MS (m/z) [M−Br]$^-$: calcd for $C_{39}H_{35}NO_2P$, 580.2; found, 580.5.

Synthesis of N,N-*di*(phenyl)-N′,N′-*di*(4-{4-N,N-*di*[4-(4-methoxyphenyl)]amino} phenyl)ethenyl-1,1′-biphenyl-4,4′-diamine (TPB-4-MOTPA)

Compound **5** (2.64 g, 4 mmol) and **3** (0.30 g, 0.5 mmol) were added into a 100 mL round-bottom flask under N_2. Anhydrous THF (40 mL) was added to above flask, cooled down to 0 °C. The THF solution of *t*BuOK (16 mmol, 0.8 mol L^{-1}) was added dropwise to above flask, stirred for 30 min at 0 °C, followed with stirred at room temperature until compound **3** was consumed completely (monitored by thin-layer chromatography). The reaction was terminate with ice water. The crude product was heated under reflux for 8 h in THF with a catalytic amount of iodine. Then the remaining iodine was removed by sodium hydroxide (NaOH) solution (Wt = 10 %, 100 mL) by stirring for 2 h. After that, the product was purified by chromatographed on a silica gel column (petroleum ether: ethyl acetate = 30:1 as eluent) to give the title compound as a pure *E* stereoisomer TPB-4-MOTPA (0.26 g, 73 %): (0.51 g, 57 %): ^{1}H NMR (400 MHz, $CDCl_3$): δ = 7.47 (d, J = 8.5 Hz, 4H, Ar H), 7.37 (d, J = 8.4 Hz, 7H, Ar H), 7.30 (d, J = 8.5 Hz, 7H, Ar H), 7.25 (s, 4H, Ar H), 7.19–7.00 (m, 28H, Ar H), 6.86 (dd, J = 26.5, 8.6 Hz, 30H), 3.80 ppm (s, 24H, OCH_3); MS (m/z) [M^-]: calcd for $C_{124}H_{104}N_6O_8$, 1805.795; found, 1805.475.

TPB-2-MOTPA was synthesized by compound **5** and **4** using the same method.

TPB-2-MOTPA (81 %): ^{1}H NMR (400 MHz, $CDCl_3$): δ = 7.42 (d, J = 8.5 Hz, 4H, Ar H), 7.31 (dd, J = 19.1, 8.6 Hz, 8H, Ar H), 7.15–6.98 (m, 24H, Ar H), 6.85 (dd, J = 28.8, 8.6 Hz, 16H, Ar H), 3.78 (s, 12H, OCH_3), 2.32 ppm (s, 6H, CH_3); MS (m/z) [M+H]$^+$: calcd for $C_{82}H_{70}N_4O_4$, 1175.540; found, 1175.837.

Quantum chemical calculation

Quantum chemical calculations were performed by using the Gaussian03 program with tBeck's three-parameter exchange

functional and Lee–Yang–Parr's correlation functional (B3LYP) using 6-31G (d) basis sets.

Device fabrication details

A 30 nm-thickness compact TiO_2 layer, 500 nm mesoporous TiO_2 layers were prepared according to the methods of our laboratory group.[8] The $CH_3NH_3PbI_3$ layer was prepared by a two-step sequential deposition method.[16] The HTMs layers were spin-coated on the top of $TiO_2/CH_3NH_3PbI_3$ films at 3000 rpm for 20 s with a concentration of 20 mg mL^{-1}. For comparison, perovskite solar cells based on *spiro*-OMeTAD were also fabricated by using a chlorobenzene solution doped with cobalt(III) bis(trifluoromethanesulfonyl)imide (Co^{III} TFSI) under the same conditions. All the above fabrication processes were carried out in air. Finally, 80 nm-thickness Au photocathode was deposited by thermal evaporation.

Acknowledgements

The authors gratefully acknowledge financial support from the National High-tech R&D Program(863 Program) (2015AA033402) and Tianjin Science and Technology Plan Projects(13ZCZDGX00900 and 14TXGCCX00017). The calculations in this work were supported by the high-performance computing center of Tianjin University, China.

Keywords: charge transfer · hole transport · hydrophobic effect · perovskites · solar cells

[1] a) Y. G. Rong, A. Y. Mei, L. F. Liu, X. Li, H. W. Han, *Acta Chim. Sin. Engl. Ed.* **2015**, *73*, 237–251; b) S. Ameen, M. A. Rub, S. A. Kosa, K. A. Alamry, M. S. Akhtar, H. S. Shin, H. K. Seo, A. M. Asiri, M. K. Nazeeruddin, *ChemSusChem* **2016**, *9*, 10; c) D. Bi, W. Tress, M. I. Dar, P. Gao, J. Luo, C. Renevier, K. Schenk, A. Abate, F. Giordano, J. P. C. Baena, J. D. Decoppet, S. M. Zakeeruddin, M. K. Nazeeruddin, M. Grätzel, A. Hagfeldt, *Sci. Adv.* **2016**, *2*, e1501170; d) H. S. Jung, N. G. Park, *Small* **2015**, *11*, 10–25.

[2] R. F. Service, *Science* **2014**, *344*, 458.

[3] a) N. J. Jeon, J. Lee, J. H. Noh, M. K. Nazeeruddin, M. Grätzel, S. I. Seok, *J. Am. Chem. Soc.* **2013**, *135*, 19087–19090; b) H. R. Li, K. W. Fu, A. Hagfeldt, M. Grätzel, S. G. Mhaisalkar, A. C. Grimsdale, *Angew. Chem. Int. Ed.* **2014**, *53*, 4085–4088; *Angew. Chem.* **2014**, *126*, 4169–4172.

[4] a) W. A. Laban, L. Etgar, *Energy Environ. Sci.* **2013**, *6*, 3249–3253; b) J. J. Shi, J. Dong, S. T. Lv, Y. Z. Xu, L. F. Zhu, J. Y. Xiao, X. Xu, H. J. Wu, D. M. Li, Y. H. Luo, *Appl. Phys. Lett.* **2014**, *104*, 063901.

[5] a) J. Liu, Y. Z. Wu, C. J. Qin, X. D. Yang, T. Yasuda, A. Islam, K. Zhang, W. Q. Peng, W. Chen, L. Y. Han, *Energy Environ. Sci.* **2014**, *7*, 2963–2968; b) P. Qin, S. Paek, M. I. Dar, N. Pellet, J. Ko, M. Grätzel, M. K. Nazeeruddin, *J. Am. Chem. Soc.* **2014**, *136*, 8516–8519; c) T. Krishnamoorthy, F. Kunwu, P. P. Boix, H. Li, T. M. Koh, W. L. Leong, S. Powar, A. Grimsdale, M. Grätzel, N. Mathews, S. G. Mhaisalkar, *J. Mater. Chem. A* **2014**, *2*, 6305–6309.

[6] a) J. A. Christians, R. C. M. Fung, P. V. Kamat, *J. Am. Chem. Soc.* **2014**, *136*, 758–764; b) S. F. Völker, S. Collavini, J. L. Delgado, *ChemSusChem* **2015**, *8*, 3012.

[7] Z. Hawash, L. K. Ono, S. R. Raga, M. V. Lee, Y. Qi, *Chem. Mater.* **2015**, *27*, 562.

[8] a) J. J. Wang, S. R. Wang, X. G. Li, L. F. Zhu, Q. B. Meng, Y. Xiao, D. M. Li, *Chem. Commun.* **2014**, *50*, 5829–5832; b) Y. Song, S. Lv, X. Liu, X. Li, S. Wang, H. Wei, D. Li, Y. Xiao, Q. Meng, *Chem. Commun.* **2014**, *50*, 15239–15242.

[9] a) Y. Shirota, H. Kageyama, *Chem. Rev.* **2007**, *107*, 953–1010; b) H. Li, K. Fu, P. P. Boix, L. H. Wong, A. Hagfeldt, M. Gratzel, S. G. Mhaisalkar, A. C. Grimsdale, *ChemSusChem* **2014**, *7*, 3420.

[10] a) W. Z. Gao, S. R. Wang, Y. Xiao, X. G. Li, *Dyes Pigm.* **2013**, *97*, 92–99; b) X. Liu, J. You, Y. Xiao, S. Wang, W. Gao, J. Peng, X. Li, *Dyes Pigm.* **2016**, *125*, 36–43.

[11] a) S. Karthikeyan, M. Thelakkat, *Inorg. Chim. Acta* **2008**, *361*, 635–655; b) I. Neogi, S. Jhulki, M. Rawat, R. S. Anand, T. J. Chow, J. N. Moorthy, *RSC Adv.* **2015**, *5*, 26806–26810; c) X. Liu, J. Liang, J. You, L. Ying, Y. Xiao, S. Wang, X. Li, *Dyes Pigm.* **2016**, *131*, 41–48.

[12] L. Zhu, J. Xiao, J. Shi, J. Wang, S. Lv, Y. Xu, Y. Luo, Y. Xiao, S. Wang, Q. Meng, X. Li, D. Li, *Nano Res.* **2015**, *8*, 1116.

[13] V. Mimaite, J. Ostrauskaite, D. Gudeika, J. V. Grazulevicius, V. Jankauskas, *Synth. Met.* **2011**, *161*, 1575–1581.

[14] X. Zhao, S. Wang, J. You, Y. Zhang, X. Li, *J. Mater. Chem. C* **2015**, *3*, 11377–11384.

[15] P. Ganesan, K. Fu, P. Gao, I. Raabe, K. Schenk, R. Scopelliti, J. Luo, L. H. Wong, M. Grätzel, M. K. Nazeeruddina, *Energy Environ. Sci.* **2015**, *8*, 1986.

[16] L. F. Zhu, J. F. Shi, S. T. Lv, Y. Y. Yang, X. Xu, Y. Z. Xu, J. Y. Xiao, H. J. Wu, Y. H. Luo, D. M. Li, Q. B. Meng, *Nano Energy* **2015**, *15*, 540–548.

[17] J. B. You, Z. R. Hong, Y. Yang, Q. Chen, M. Cai, T. B. Song, C. C. Chen, S. R. Lu, Y. S. Liu, H. P. Zhou, *ACS Nano* **2014**, *8*, 1674–1680.

[18] H. P. Zhou, Q. Chen, G. Li, S. Luo, T.-B. Song, H.-S. Duan, Z. N. Hong, J. B. You, Y. S. Liu, Y. Yang, *Science* **2014**, *345*, 542–546.

[19] N. H. Tiep, Z. Ku, H. J. Fan, *Adv. Energy Mater.* **2016**, *6*, 1501420.

[20] J. L. Yang, B. D. Siempelkamp, D. Y. Liu, T.-L. Kelly, *ACS Nano* **2015**, *9*, 1955–1963.

[21] H.-S. Kim, C.-R. Lee, J.-H. Im, K.-B. Lee, T. Moehl, A. Marchioro, S.-J. Moon, R. Humphry-Baker, J.-H. Yum, J. E. Moser, M. Grätzel, N.-G. Park, *Sci. Rep.* **2012**, *2*, 591.

[22] X. Z. Guo, Y. H. Luo, Y. D. Zhang, X. C. Huang, D. M. Li, Q. B. Meng, *Rev. Sci. Instrum.* **2010**, *81*, 103106.

[23] A. P. Cote, M. A. Heuft, US 7652148 Bl, **2010**.

Received: May 11, 2016
Revised: May 13, 2016
Published online on June 15, 2016

